Arm Voltage Estimation Method for Compensated Modulation of Modular Multilevel Converters

Abel A. Taffese
Elisabetta Tedeschi
Dept. of Electric Power Engineering
Norwegian University of Science and Technology
Trondheim, Norway
abel.taffese@ntnu.no, elisabetta.tedeschi@ntnu.no

Erik de Jong
Dept. of Electrical Engineering
Technische Universiteit Eindhoven
Eindhoven, The Netherlands
e.c.w.de.jong@tue.nl

***Abstract*—The Modular Multilevel Converter (MMC), being a complex system, requires a number of controllers to function properly. These range from low level switching pattern generation to high level control loops. Among these controllers are modulation techniques that calculate the insertion indices, control inputs that decide the number of sub-modules inserted in a given arm. One such technique is compensated modulation which divides the reference voltages, generated by high level controllers, by the respective arm voltages (sum of capacitor voltages) when calculating the insertion indices. This prevents the arm voltage ripple from affecting the generated output voltage. For this purpose, the arm voltages can be measured (closed-loop approach) or estimated (open-loop approach). This paper presents an arm voltage estimation technique for compensated modulation of MMCs. The proposed technique combines the benefits of the open-loop approach with that of the closed loop one.**

***Index Terms*—Energy control, open-loop, closed-loop, MMC, Modulation, Voltage estimation, Compensated modulation**

I. Introduction

The Modular Multilevel Converter (MMC) is arguably one of the most complex power converters ever built. It consists of hundreds of Sub-Modules (SMs) when used in HVDC applications. It has attracted a lot of research activity in recent years. One of the research areas is the development of modulation techniques which are strategies to select the number of modules inserted in a given arm at a given time. Outputs of these techniques are insertion indices. Among the modulation techniques proposed [1], direct modulation is the simplest. However, an MMC operating under direct modulation exhibits substantial harmonic components in the circulating current because it does not account for the ripples in the SM capacitor voltages and the voltage drop on the arm inductance. A better alternative is to use compensated modulation [2], [3]. Compensated modulation avoids unwanted harmonics from the circulating current by accounting for the ripple in the sum of the capacitor voltages (henceforth referred to as *arm voltages*). This is achieved by dividing the reference voltages by the respective arm voltages during the calculation of the insertion indices [2]. This prevents arm voltage ripple from distorting the generated voltage and hence the circulating current can be controlled to have only a dc component. However, there are two challenges with this approach; (1) arm voltage measurement delay and (2) loss of inherent stability of the arm energy [4]. Ref. [4] proposed an open-loop approach to overcome these challenges. This approach was later proven to be globally asymptotically stable [5] and extended to include current control [6]. A shortcoming of this approach is that it relies on accurate knowledge of parameters, such as capacitance. Parameter errors can significantly impact its normal operation. On-line estimation of parameters is proposed in [6] to counter this shortcoming.

This paper proposes an alternative approach that uses the average component of the measured arm voltage to close the energy control loop. The main difficulties with arm voltage measurement are distortion and delay. But, these only affect the ripple and not the average components. So, the measurement can be filtered and the average component can be used in a closed loop controller. The ripple, on the other hand, will be estimated from a closed form expression. This approach combines the inherent stability of the open-loop approach with reduced parameter sensitivity of the closed loop one.

The rest of this paper is organized as follows. Section II presents the basic energy dynamic equations followed by derivation of the arm voltage estimator in Section III. Implementation details are described in Section IV. Then analysis of system is presented in Section V followed by simulation results in Section VI.

II. Energy Dynamics

The equations in this section closely follow the nomenclature in [7]. The symbols can be read from Fig. 1. All the equations are per-phase and in per-unit to the bases given in the Appendix. The ac voltages and currents are normalized with ac base values while the remaining quantities are divided by the dc side base values. The base value for the arm energy is defined in such a way that $W_{arm} = v_{arm}^2$ in per-unit [3] where W_{arm} and v_{arm} are the arm energy and voltage, respectively. For large number of sub-modules [7], insertion indices of the upper and lower arms can be approximated by continuous

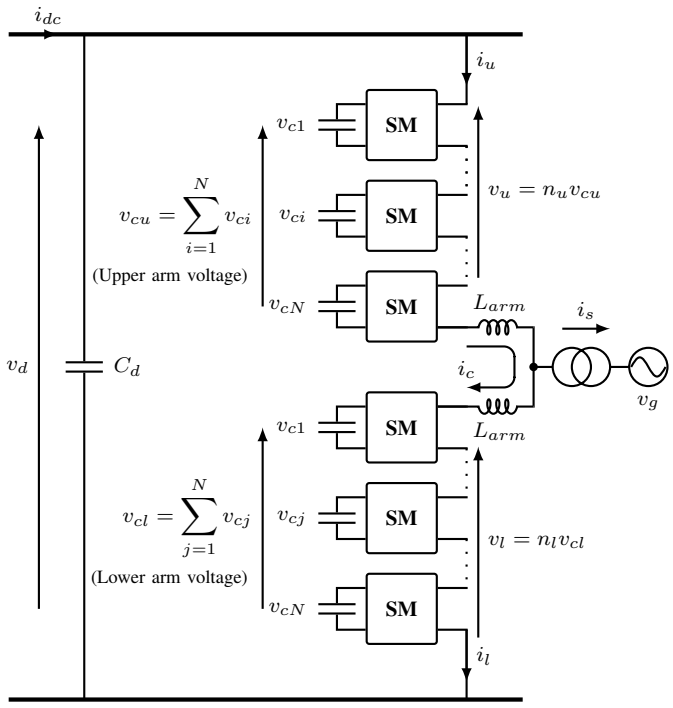

Fig. 1. Per-phase MMC circuit diagram.

signals, (1).

$$\begin{aligned} n_u &= \frac{1}{\hat{v}_{cu}} \left(\frac{1}{2} v_d^* - v_c^* - \frac{1}{2} v_s^* \right) \\ n_l &= \frac{1}{\hat{v}_{cl}} \left(\frac{1}{2} v_d^* - v_c^* + \frac{1}{2} v_s^* \right) \end{aligned} \tag{1}$$

where v_d^*, v_c^*, and v_s^* are reference values for dc, common mode, and ac voltages, respectively. $\hat{v}_{cu}$ and $\hat{v}_{cl}$ are estimates of the upper and lower arm voltages. The insertion indices will effectively be multiplied by the actual arm voltages to obtain the inserted voltages v_u and v_l. Hence, the dynamics of energy stored in the upper and lower arms is given by (2) where c_p is the per-unit equivalent arm capacitance in seconds.

$$\begin{aligned} \frac{\mathrm{d}}{\mathrm{d}t} W_u &= \frac{2}{c_p} i_u v_u = \frac{2}{c_p} i_u \frac{v_{cu}}{\hat{v}_{cu}} \left(\frac{1}{2} v_d^* - v_c^* - \frac{1}{2} v_s^* \right) \\ \frac{\mathrm{d}}{\mathrm{d}t} W_l &= \frac{2}{c_p} i_l v_l = \frac{2}{c_p} i_l \frac{v_{cl}}{\hat{v}_{cl}} \left(\frac{1}{2} v_d^* - v_c^* + \frac{1}{2} v_s^* \right) \end{aligned} \tag{2}$$

where W_u and W_l are the energy stored in the upper and lower arms. i_u and i_l are the upper and lower arm currents. These currents can be decomposed in to common mode, i_c, and differential mode components, i_s [7]. Applying this decomposition, the upper and lower arm energy equations can be written as (3) and (4), respectively.

$$\frac{\mathrm{d}}{\mathrm{d}t} W_u = \frac{2}{c_p} \frac{v_{cu}}{\hat{v}_{cu}} \left(\frac{1}{2} v_d^* - v_c^* - \frac{1}{2} v_s^* \right) \left(i_c + \frac{2}{3} i_s \right) \tag{3}$$

$$\frac{\mathrm{d}}{\mathrm{d}t} W_l = \frac{2}{c_p} \frac{v_{cl}}{\hat{v}_{cl}} \left(\frac{1}{2} v_d^* - v_c^* + \frac{1}{2} v_s^* \right) \left(i_c - \frac{2}{3} i_s \right) \tag{4}$$

The circulating current, i_c, dynamics is given by (5).

$$\begin{aligned} l_d \frac{\mathrm{d}}{\mathrm{d}t} i_c = \frac{1}{2} v_d &- \frac{1}{2} \left(\frac{v_{cu}}{\hat{v}_{cu}} + \frac{v_{cl}}{\hat{v}_{cl}} \right) \left(\frac{1}{2} v_d^* - v_c^* \right) \\ &+ \frac{1}{2} \left(\frac{v_{cu}}{\hat{v}_{cu}} - \frac{v_{cl}}{\hat{v}_{cl}} \right) v_s^* - r_d i_c \end{aligned} \tag{5}$$

where l_d and r_d are per unit arm inductance and resistance referred to the dc base values. Eqs. (3) to (5) represent detailed third order energy dynamics of the MMC. Simplifications will be made to these expressions in the derivation and analysis of the estimation technique in subsequent sections.

III. Arm Voltage Estimator

The main goal of the estimator is to provide an output that will closely follow the measured value while fulfilling two additional requirements; (1) Error in parameter value should not critically affect the system, and (2) Average part of the arm energy should be closed-loop controlled with good dynamic response. The first requirement implies that if there are errors in parameters, such as arm capacitance, the converter should continue to operate normally with a slight reduction in performance at worst. The second requirement enforces consistent dynamic behaviour under various operating conditions. Both requirements are fulfilled by incorporating average energy controller as will be shown in subsequent sections.

The following simplifying assumptions are made in the derivation of the arm voltage estimator.

1) The ac side quantities are pure fundamental frequency sinusoids as shown in (6) and (7).

$$i_s = \hat{i}_s \cos\left(\omega t + \phi_i\right) \tag{6}$$

$$v_s^* = \hat{v}_s^* \cos\left(\omega t + \phi_v\right) \tag{7}$$

   where $\hat{i}_s$ and $\hat{v}_s^*$ are peaks values of the ac current and internal ac voltage reference, respectively. ϕ_i and ϕ_v are phase angles of the ac current and voltage, respectively, with respect to a common reference. ω is the fundamental frequency in rad/sec.
2) The quantities $\hat{i}_s$, $\hat{v}_s^*$, v_d^*, v_c^*, and i_c are assumed not to change abruptly within a fundamental period, $20ms$. Therefore, they are considered to be constants in this derivation.
3) A balanced symmetric three phase system is considered in this paper.
4) The estimates of arm voltages closely follow the actual ones. So they can be considered to be equal.

Assumptions 1 to 3 are reasonable for grid connected applications. The last assumption is claiming that the estimator is ideal. While this is fine for the calculation of closed form expression, it has a subtle consequence on the control tuning. This will be investigated in Section V. With these assumptions and equations, closed form expressions, (8) and (9), for arm

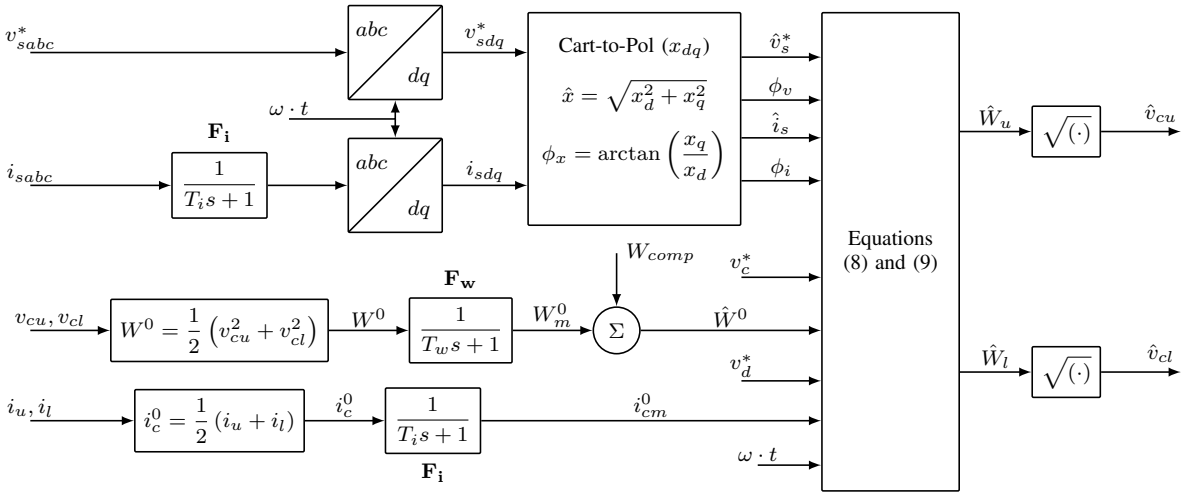

Fig. 2. Block diagram of the proposed arm voltage estimation method.

energies can be derived by substituting (6) and (7) in (3) and (4), and performing integration similar to [5].

$$\hat{W}_u = W_0 + \frac{2}{\omega c_p}\Bigg[+ \frac{2}{3}\left(\frac{1}{2}v_d^* - v_c^*\right)\hat{i}_s \sin(\omega t + \phi_i) - \frac{1}{12}\hat{v}_s^*\hat{i}_s \sin(2\omega t + \phi_i + \phi_v) - \frac{1}{2}\hat{v}_s^* i_c \sin(\omega t + \phi_v)\Bigg] \tag{8}$$

$$\hat{W}_l = W_0 + \frac{2}{\omega c_p}\Bigg[- \frac{2}{3}\left(\frac{1}{2}v_d^* - v_c^*\right)\hat{i}_s \sin(\omega t + \phi_i) - \frac{1}{12}\hat{v}_s^*\hat{i}_s \sin(2\omega t + \phi_i + \phi_v) + \frac{1}{2}\hat{v}_s^* i_c \sin(\omega t + \phi_v)\Bigg] \tag{9}$$

W_0 is the average component of the arm energies. $\hat{W}_u$ and $\hat{W}_l$ are estimated energies of the upper and lower arms, respectively. Extension to three phase is a matter of adding appropriate phase shifts since the system is balanced. Equations (8) and (9) are identical to the ones derived in [5] with some minor difference in the phase angle notation, and scaling factors due to the per-unit convention followed in this paper. The main differences between the proposed estimator and the one in [5] are on the calculation of the average component and implementation details which are discussed in the next section.

IV. Implementation

Under ideal conditions, i.e. all the parameters accurately known and all the signals instantaneously available, the arm energies can be perfectly estimated using (8) and (9) as was shown in [4], [5], [7]. However, there will inevitably be parameter errors and measurement lags in practical systems. The approach followed in this paper aims to exploit the measurements already available in achieving reduced sensitivity to parameter variations and compensate for measurement lags. This is done by closing the energy control loop using average component of the arm voltage measurement. In this way the average component will not be affected by parameter variation. The complete scheme is shown in Fig. 2. The average value is extracted by passing the arm energies through a low-pass filter. The phase angle reference, ωt, is obtained from a Phase Locked Loop (PLL). Filter lag compensations and control design are presented in the following sections.

A. Filter Compensation

First order measurement filters are included in the block diagram, (Fig. 2), to represent anti-aliasing and smoothing filters that are present in practical implementations. These filters result in phase and gain change in the ac signals. Under steady-state and slowly changing conditions, these can be compensated for by simple gain and phase compensation as shown in (10) and (11), respectively. A similar approach can be applied to compensate for communications delays on the signals.

$$G_{comp} = \sqrt{(\omega T_x)^2 + 1} \tag{10}$$

$$\phi_{comp} = \arctan(\omega T_x) \tag{11}$$

where T_x is the filter time constant and ω is the ac frequency. G_{comp} multiplies the signal magnitude after the filter and ϕ_{comp} gets added to the phase angle. Uncertainty in T_x and ω might prevent prefect compensation. However, as will be shown in Section VI, its impact is not significant.

B. Control Design

A simplified model shown in Fig. 3, based on the assumptions in Section III and equations (3) to (5), is used for control design. It is assumed that $(v_d^* - 2v_c^*) \approx v_d^*$ which is reasonable under normal operation. The boldface letters above the blocks will be used to refer to the transfer functions. This structure

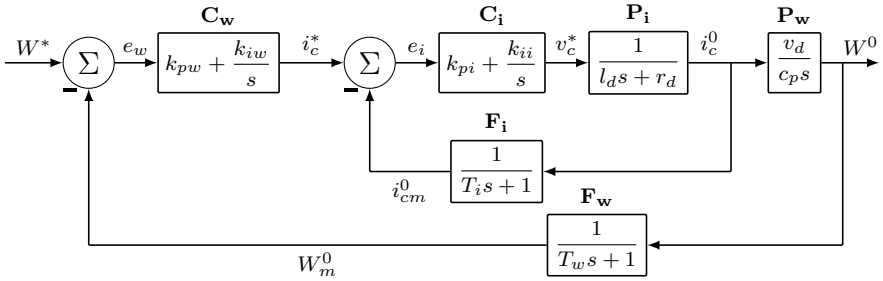

Fig. 3. Energy and circulating current control loops.

is well suited for Modulus and Symmetric optimum tuning techniques [8]. $\mathbf{C_i}$ is tuned using modulus optimum while $\mathbf{C_w}$ is designed using symmetric optimum method.

V. Analysis

The analysis in this section is performed to study the effect of assuming that the estimator is ideal (assumption (4) Section III). In order to simplify the analysis, only the average components will be considered. Furthermore, the difference in average energies between the upper and lower arms is considered to be zero following a similar argument as [7]. This permits the simplification in (12).

$$\frac{v_{cu}}{\hat{v}_{cu}} \approx \frac{v^0}{\hat{v}^0} \approx \frac{v_{cl}}{\hat{v}_{cl}} \tag{12}$$

where v^0 and $\hat{v}^0$ are average components of the actual and estimated voltages. Taking this into consideration and averaging the arm energies results in (13) and (14) where W^0 is the average energy.

$$\frac{\mathrm{d}}{\mathrm{d}t}W^0 = \frac{2}{c_p}\frac{v^0}{\hat{v}^0}\left[\left(\frac{1}{2}v_d^* - v_c^*\right)i_c - \frac{1}{3}v_s^* i_s\right] \tag{13}$$

$$l_d\frac{\mathrm{d}}{\mathrm{d}t}i_c = \frac{1}{2}v_d - \frac{1}{2}\frac{v^0}{\hat{v}^0}v_d^* + \frac{v^0}{\hat{v}^0}v_c^* - r_d i_c \tag{14}$$

Substituting the arm voltages, v^0 and $\hat{v}^0$ with the corresponding energies,$\sqrt{W^0}$ and $\sqrt{\hat{W}^0}$, and linearising (13) and (14) around a steady state operating point gives (15) and (16).

$$\frac{\mathrm{d}}{\mathrm{d}t}W^0 = \frac{2}{c_p}\left[\left(\frac{1}{2}v_d^* - v_c^*\right)i_c - \frac{1}{3}v_s^* i_s\right] \tag{15}$$

$$l_d\frac{\mathrm{d}}{\mathrm{d}t}i_c = v_c^* - r_d i_c - k\left(W^0 - \hat{W}^0\right) \tag{16}$$

where k is a positive linearisation constant. It can be seen that there is an equivalent proportional energy controller with gain k inherently in the system. This fact is the foundation of the open-loop approach. The parameter k is a function of system parameters and initial conditions. Therefore, the convergence speed cannot be controlled. To solve this problem, a closed loop control is needed. First, the current controller, $\mathbf{C_i}$ from Fig. 3, is incorporated to the linear model of (15) and (16). In doing so, the transfer function from current reference, i_c^* to the average energy, W^0, becomes:

$$\frac{W^0}{i_c^*} = \frac{v_d\mathbf{P_i}\mathbf{C_i}}{c_p s\left(1 + \mathbf{P_i}\mathbf{C_i}\mathbf{F_i}\right) + k\left(1 - \mathbf{G}\right)\mathbf{P_i}} \tag{17}$$

where $\mathbf{G}$ is a transfer function relating $\hat{W}^0$ to W^0, i.e. $\hat{W}^0 = \mathbf{G}W^0$. When $\mathbf{G} = 1$, (17) reduces to the transfer function obtained from the block diagram of Fig. 3. Therefore, the controller design presented in Section IV-B is valid only when $\mathbf{G} = 1$. This will affect the controller performance and will be addressed here. From (Fig. 2) and definition of $\mathbf{G}$, the relation in (18) can be found.

$$\hat{W}^0 = \mathbf{F_w}W^0 + W_{comp} = \mathbf{G}W^0 \tag{18}$$

where W_{comp} is compensation signal to improve the controller performance. $\mathbf{F_w}$ is the energy filter transfer function, (Fig. 3). The value of W_{comp} that will result in $\mathbf{G} = 1$ is given in (19). This is equivalent to computing the derivative of W^0 multiplying it by the energy filter time constant, T_w, and passing it through the energy filter.

$$W_{comp} = \left(1 - \mathbf{F_w}\right)W^0 = T_w s W^0 \mathbf{F_w} \tag{19}$$

However, computing direct derivative leads to noise amplification. So a better alternative is to estimate the derivative using measurement already available. In such a way the complete compensation signal is given by (20).

$$W_{comp} = \frac{2T_w}{c_p}\left[\left(\frac{1}{2}v_d^* - v_c^*\right)i_c - \frac{1}{12}\hat{v}_s^*\hat{i}_s\cos(\phi_i - \phi_v)\right]\cdot\mathbf{F_w} \tag{20}$$

This value of W_{comp} will cancel the effect of the energy filter and improve performance of the controller. The next section will present simulation results that support this analysis.

VI. Simulation Results

Simulation results showing performance of the proposed method are presented in this section. The system under test is a three phase MMC HVDC terminal connected to a droop (1%) controlled dc bus and a strong ac grid via a transformer. The simulation is performed in Matlab/SIMULINK environment. The parameters, Table I, and the modelling approach are adopted from [9]. The dc voltage reference is set at $v_d^* = 1.0$. The average arm voltage is set to 15% above the nominal dc voltage to account for redundant sub-modules. The results show the effect of: (1) energy filter compensation, (2) ac filter lag compensation, and (3) parameter error in capacitance value. The simulation includes two disturbances, (1) a step change in energy reference from $W^* \approx 1.31$ to $W^* \approx 1.18\,pu$ at $t = 2$ sec, and (2) a step change in ac power from

TABLE I
PARAMETERS USED FOR SIMULATION

Parameter	Value
Base apparent power, S_b	900 MVA
Base dc voltage, V_b^{dc}	640 kV
Frequency, ω	$2\pi 50$ rad/s
Arm capacitance, C_{arm}	29 μF
Arm inductance, L_{arm}	84 mH
Arm resistance, R_{arm}	0.885 Ω
Transformer reactance, X_t	17.7 Ω
Transformer resistance, R_t	1.77 Ω
Voltage filter time constant, T_v	500 μs
Current filter time constant, T_i	500 μs
Energy filter time constant, T_w	10 ms
Energy controller proportional constant, k_{pw}	13.6
Energy controller integral constant, k_{iw}	0.6
Circ. current controller proportional constant, k_{pcc}	0.046
Circ. current controller integral constant, k_{icc}	0.486
Simulation time step, T_{sim}	100 μs
Controller sampling time, T_s	200 μs

*Circ. = Circulating.

0.89 pu (800 MW) to 0.45 pu (400 MW) at $t = 7$ sec. Fig. 4 shows a result of the basic implementation by using (8)

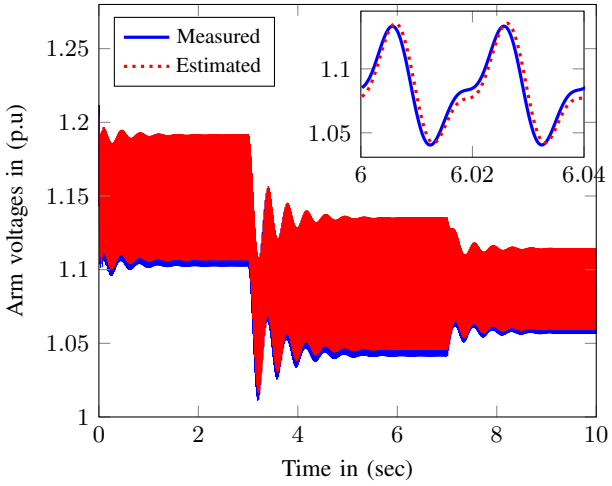

Fig. 4. Arm voltage using the basic implementation of (8) and (9)

and (9) directly. The average energy exhibits poorly damped oscillation. As discussed in Section V, this is caused by the lag in the energy filter, T_w. It can be effectively damped by applying the energy filter compensation proposed in the previous section, Fig. 5. As can be seen from the insets of Figs. 4 and 5 there is a clearly visible time delay in the estimated signal which is caused by the ac filters, T_i and T_v. As proposed in Section IV, a steady-state compensation for the filter gains and phases is applied to obtain the result in Fig. 6 where the measured and estimated values are well matched. Effect of error in capacitance value is displayed in Figs. 7 and 8 where the considered value is 20% lower than the actual one. Despite a slight reduction damping, the average energy is not affected by the parameter error, (Fig. 8). The effect is visible on the circulating current, Fig. 9. The error has caused as second harmonic circulating current with a magnitude

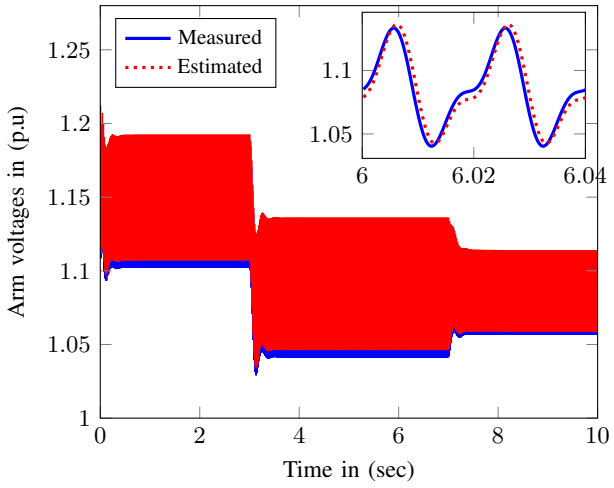

Fig. 5. Arm voltage after applying energy filter compensation

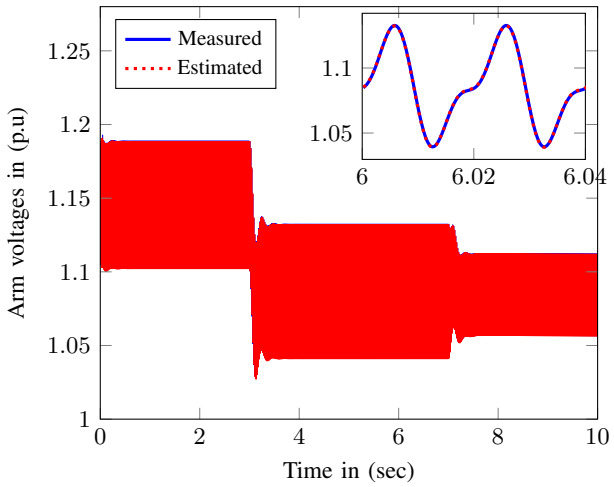

Fig. 6. Arm voltage after applying both energy and ac filter compensations

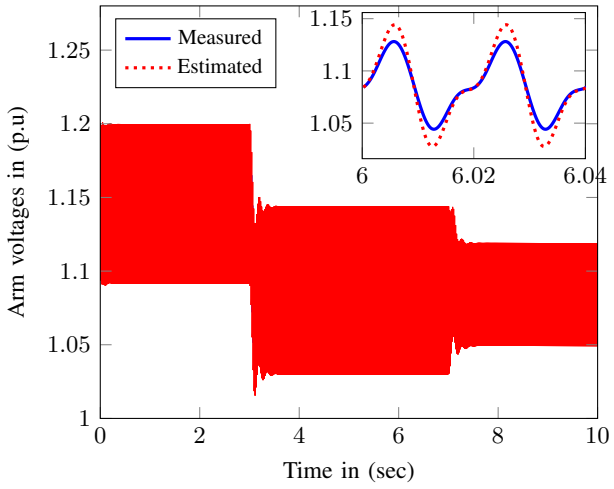

Fig. 7. Arm voltage after applying both energy and ac filter compensations and 20% parameter error in capacitance

approximately 30% of the dc value. The ripple is also present when the ac filter delays are not compensated, Fig. 9. The 80% compensation case shows the impact of uncertainty in T_i when it is known within ±20%. The result shows ±20% that uncertainty in time constant does not significantly affect the ripple in the circulating current. However, ignoring delays caused significant ripple in the circulating current. Fig. 10 shows ac power and dc voltage signal when there is parameter error. This confirms that the converter continues to operate normally when parameter error occurs.

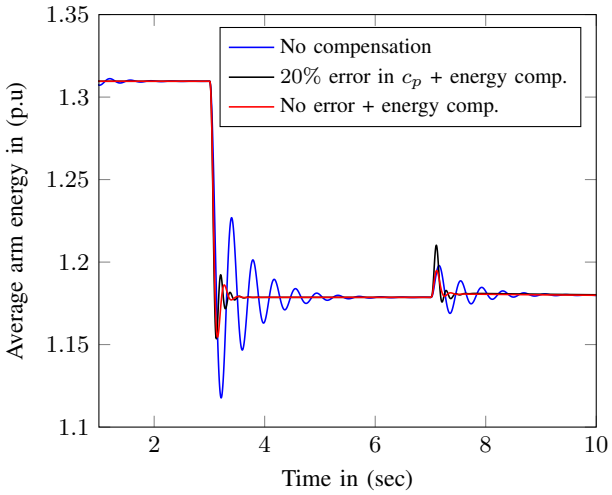

Fig. 8. Impact of compensation and parameter error on average arm energy.

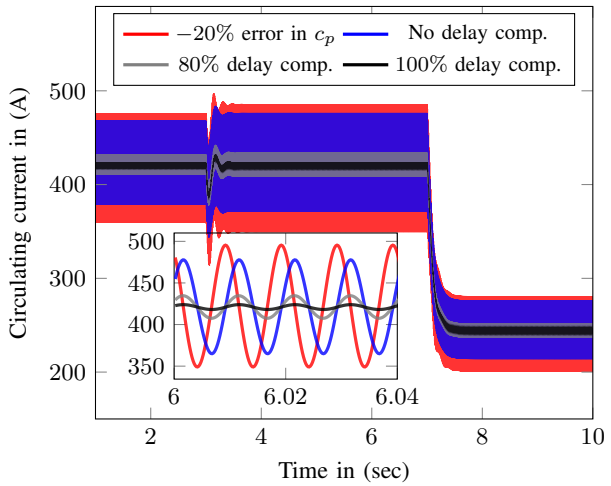

Fig. 9. Circulating current under 20% parameter error in capacitance and different levels of delay compensation.

VII. Conclusion

This paper proposes a technique for estimating the arm voltage to be used for compensated modulation. Derivation and analysis presented in this paper are supported by simulation results. The technique considers measurement filters and the corresponding compensation required for successful

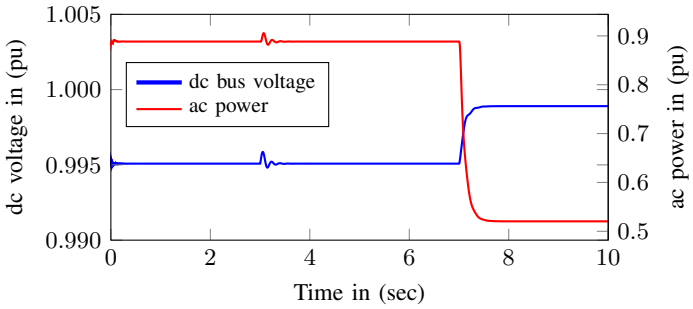

Fig. 10. dc voltage and ac power when operating with 20% parameter error in capacitance.

estimation of the arm voltage. A compensation scheme that avoids the impact of the delay introduced by the energy filter has also been proposed and verified via simulation. The results have shown that the estimator has very promising performance both under normal conditions and with parameter errors. However, further development is needed to avoid the ripple when operating with parameter error.

Appendix

The base values used for per-unit calculations are depicted in (21).

$$I_b^{ac} = \frac{2S_b}{3V_b^{ac}} \quad Z_b^{ac} = \frac{V_b^{ac}}{I_b^{ac}} \quad I_b^{dc} = \frac{S_b}{V_b^{dc}} \quad Z_b^{dc} = \frac{V_b^{dc}}{I_b^{dc}}$$
$$L_b^{ac} = Z_b^{ac} \quad C_b^{ac} = \frac{1}{Z_b^{ac}} \quad L_b^{dc} = Z_b^{dc} \quad C_b^{dc} = \frac{1}{Z_b^{dc}}$$
$$V_b^{dc} = 2V_b^{ac} \quad W_b = \frac{1}{2}C_b^{dc}\left(V_b^{dc}\right)^2 \tag{21}$$

References

[1] S. Debnath, J. Qin, B. Bahrani, M. Saeedifard, and P. Barbosa, "Operation, control, and applications of the modular multilevel converter: A review," *IEEE Trans. Power Electron.*, vol. 30, no. 1, pp. 37–53, Jan. 2015.

[2] A. Antonopoulos, L. Angquist, and H. P. Nee, "On dynamics and voltage control of the modular multilevel converter," in *Proc. 13th European Conf. Power Electronics and Applications EPE '09*, Sep. 2009, pp. 1–10.

[3] G. B. Diaz, J. A. Suul, and S. D'Arco, "Small-signal state-space modeling of modular multilevel converters for system stability analysis," in *Proc. IEEE Energy Conversion Congress and Exposition (ECCE)*, Sep. 2015, pp. 5822–5829.

[4] L. Ängquist, A. Haider, H. P. Nee, and H. Jiang, "Open-loop approach to control a modular multilevel frequency converter," in *Proc. 2011-14th European Conf. Power Electronics and Applications (EPE 2011)*, Aug. 2011, pp. 1–10.

[5] A. Antonopoulos, L. Ängquist, L. Harnefors, K. Ilves, and H. P. Nee, "Global asymptotic stability of modular multilevel converters," *IEEE Trans. Ind. Electron.*, vol. 61, no. 2, pp. 603–612, Feb. 2014.

[6] L. Harnefors, A. Antonopoulos, K. Ilves, and H. P. Nee, "Global asymptotic stability of current-controlled modular multilevel converters," *IEEE Trans. Power Electron.*, vol. 30, no. 1, pp. 249–258, Jan. 2015.

[7] L. Harnefors, A. Antonopoulos, S. Norrga, L. Angquist, and H. P. Nee, "Dynamic analysis of modular multilevel converters," *IEEE Trans. Ind. Electron.*, vol. 60, no. 7, pp. 2526–2537, Jul. 2013.

[8] J. W. Umland and M. Safiuddin, "Magnitude and symmetric optimum criterion for the design of linear control systems: what is it and how does it compare with the others?" *IEEE Transactions on Industry Applications*, vol. 26, no. 3, pp. 489–497, May 1990.

[9] W. Leterme, N. Ahmed, J. Beerten, L. Angquist, D. V. Hertem, and S. Norrga, "A new hvdc grid test system for hvdc grid dynamics and protection studies in emt-type software," in *11th IET International Conference on AC and DC Power Transmission*, Feb 2015, pp. 1–7.